A catalytically silent FAAH-1 variant drives anandamide transport in neurons

Jin Fu[1¶], Giovanni Bottegoni[2¶], Oscar Sasso[2], Rosalia Bertorelli[2], Walter Rocchia[2], Matteo Masetti[2], Ana Guijarro[1], Alessio Lodola[3], Andrea Armirotti[2], Gianpiero Garau[2], Tiziano Bandiera[2], Angelo Reggiani[2], Marco Mor[3], Andrea Cavalli[2,4], Daniele Piomelli[1,2*]

Supplementary Material

Supplementary Figure Legends

Supplementary Fig. 1. Identification of FLAT in rat and mouse tissues. (**a-c**) Reverse transcriptase-polymerase chain reaction (RT-PCR) analyses show the presence of FLAT transcript (bottom band) in various rat brain regions (**a**), rat tissues (**b**) and neural cells (**c**). The top band is the FAAH-1 transcript. Both bands were identified by nucleotide sequencing. (**d**) Ribonuclease protection assays showing the presence of FLAT mRNA (left panel) and FAAH-1 mRNA (right panel) in rat brain and liver. (Lane 1) Radioactive probe digested with T1 ribonuclease; (lane 2) Undigested probe; (lane 3) T1 ribonuclease digestion after hybridization with rat brain mRNA; (lane 4) T1 ribonuclease digestion after hybridization with rat liver mRNA. Top arrows indicate the position of the radioactive probe; bottom arrows indicate the position of the hybridized product. (**e**) Southern blot analyses of cDNA generated by reverse transcription of total RNA extracted from rat brain (lane 1) or liver (lane 2). We hybridized blots with radioactive probes complementary to either the 3'- or 5'-terminus of FAAH-1. The 3'-probe recognized only one band, corresponding to FAAH-1 cDNA, whereas the 5'-probe

recognized two bands, corresponding to FAAH-1 cDNA (top) and FLAT cDNA (bottom). (**f**) Quantitative RT-PCR analyses of FAAH-1 mRNA (open bars) and FLAT mRNA (closed bars) in various regions of the rat brain. Abbreviations: Ctx, cortex; Hipp, hippocampus; Stri, striatum; Thal, thalamus; Hypo, hypothalamus; Cere, cerebellum; BS, brainstem. (**g**) Western blot analysis of membrane protein extracts (membrane) and cytosolic protein extracts (cytosol) from liver (lane 1) or brain (lane 2) of wild-type C57/Bl6 mice (wt) or FAAH-1-deficient mice ($FAAH^{-/-}$). Numbers on the left of the gel indicate molecular weight markers (in kD) and apparent molecular weights of FAAH-1 (65 kD) and FLAT (56 kD).

Supplementary Fig. 2. Hydrolysis of various radioactively labeled lipids by extracts of vector-transfected Hek293 cells (open bars), FLAT-expressing Hek293 cells (closed bars) or FAAH-1-expressing Hek293 cells (shaded bars). Hydrolysis of (**a**) [^{3}H]-anandamide; (**b**) [^{3}H]-oleoylethanolamide (OEA); (**c**) [^{3}H]-2-oleoyl-*sn*-glycerol (2-OG). Amidase and esterase activities were assayed as described in Supplementary Methods. Results are expressed as mean ± SEM of 5-6 separate experiments. ***, $P<0.001$ versus vector control, ANOVA followed by Dunnett's test.

Supplementary Fig. 3. Enhanced flexibility of the α2-interacting loop may increase access of water to the substrate-binding pocket of FLAT. The bottom panel shows changes in average water coordination of the side-chain nitrogen in Lys^{142} (blue line, left y axis) and the χ1 dihedral value of Met^{191} (red line, right y axis) as a function of simulated time. Met^{191} participates in substrate binding by accepting on its backbone carbonyl a hydrogen bond from the amide nitrogen of anandamide. Furthermore, its side chain may gate the access of water through the cytosolic channel to the catalytic pocket. Gray areas in the plot highlight two different regimes of water coordination; the last

configuration in each regime is displayed in the top panels, which show a detail of the catalytic site of FLAT (white ribbons) together with the α2 helix (transparent orange ribbons) of FAAH-ΔTM, after superposition of the common core of the two proteins. The α2-interacting loop is shown in violet. The catalytic triad (Ser^{217}, Lys^{142} and nucleophile Ser^{241}) and Met^{191} are shown as a licorice model. For each configuration, the overall displacement from the starting structure (corresponding to the end of the thermalization) of flexible residues belonging to the α2-interacting loop and the catalytic region is shown with red arrows, with the length of each arrow proportional to the calculated displacement. The solvation in proximity of Lys^{142} is shown by using transparent blue isocontour surfaces representing the average number of water molecules in each window (~1 in the left window, ~3 in the right window). The blue sphere in the right window symbolizes a water molecule that has a high probability of being found in that position.

Supplementary Fig. 4. Electrostatic potential differences between FLAT and FAAH-1. Superimposition of representative structures taken from Molecular Dynamics simulations of FAAH-ΔTM and FLAT (white ribbons). The α2 helix of FAAH-ΔTM is shown in orange and a clipping plane passing through catalytic triad residue Lys^{142} is represented and colored according to the difference between the electrostatic potential generated by FLAT and FAAH-ΔTM. Blue and red color codes correspond to positive and negative potential differences, respectively. Lys^{142} is located in an area that displays an overall negative potential difference.

Supplementary Fig. 5. Gel filtration analysis of recombinant FLAT. The purified protein runs as a single band on denaturing SDS-PAGE gels with an apparent molecular weight of 56 kDa, and elutes from size exclusion chromatography at a retention volume

corresponding to a molecular mass of 120 kDa. These results suggest that FLAT is a homodimer in aqueous solution.

Supplementary Fig. 6. Subcellular localization of recombinant FLAT and FAAH-1 in extracts of Hek293 cells. (**a**) We fractionated cell extracts by ultracentrifugation and subjected the fractions to western blot analyses using antibodies for V5 (top) and β-actin (bottom): (1) cytosolic fraction; (2) membrane fraction. After treating membranes with Na_2CO_3 (0.1 M), we separated soluble (3) and insoluble (4) protein fractions and analyzed them by western blot. Bands were visualized by electrochemiluminescence. (**b**) We quantified band intensities using the National Institutes of Health Image software, with β-actin as an internal standard. Results are expressed as mean ± SEM of 3 separate experiments.

Supplementary Fig. 7. Over-expression of FLAT enhances anandamide release from Neuro-2A cells. Levels of anandamide (**a**), 2-AG (**b**) and OEA (**c**) were measured by liquid chromatography/mass spectrometry in culture media of Neuro-2A cells over-expressing vector control (open bars) or FLAT (closed bars). ***, $P<0.001$ versus vector control, Student's *t*-test. n = 5.

Supplementary Fig. 8. Funnel plot summarizing the stepwise virtual ligand-screening process. Compounds were selected from the Molcart database (Molsoft, LaJolla, California). At each stage, an increasingly severe filtering procedure was applied to prioritize compounds while preserving chemical diversity.

Supplementary Fig. 9. Uptake of [^{3}H]-anandamide (AEA) in brain neurons from FAAH-deficient mice. Effect of vehicle (0.01% DMSO), or ARN272 (10 μM) on [^{3}H]-anandamide

uptake in brain primary cultures of wild-type (open bars) or *faah*$^{-/-}$ mice (closed bars). Neurons were incubated with [^{3}H]-anandamide for 5 min at 37°C and internalization measured as described in Supplementary Methods. Results are expressed as mean ± SEM of 4 separate experiments. **, P<0.01 versus vehicle control, ANOVA followed by Dunnett's test.

Supplementary Fig. 10. Effects of the FLAT inhibitor ARN272 (μM) on the activities of various endocannabinoid-metabolizing enzymes and cannabinoid receptor binding: (**a**) rat brain *N*-acylphosphatidylethanolamine-specific phospholipase D (NPLD); (**b**) recombinant rat monoacylglycerol lipase (MGL); (**c**) recombinant rat diacylglycerol lipase-α (DGL-α); (**d**) recombinant rat *N*-acylethanolamide-hydrolysing acid amidase (NAAA); (**e**) [^{3}H]-CP55940 or [^{3}H]-anandamide binding to rat brain membranes. Binding is significantly inhibited by the cannabinoid agonist Win-55212. [^{3}H]-anandamide binding was measured in the presence of FAAH inhibitor URB597 (1 μM). **, P<0.01 versus vehicle control, n=4.

Supplementary Fig. 11. Central antinociceptive effects of ARN272 on formalin-induced pain in mice. Administration of ARN272 (μg, i.c.v) dose-dependently reduced nocifensive behavior in both phase I (0-5 min) and phase II (5-45 min), after intraplantar formalin injection (5%, 20 μl). Results are expressed as the mean ± SEM of 6 mice per group. ***, P<0.001 versus control; two-way ANOVA followed by Bonferroni's test.

Supplementary Fig. 12. Antinociceptive effects of ARN272 0h and 4 h after intraplantar injection of carrageenan. Administration of ARN272 (mg-kg^{-1}, i.p.) reduced carrageenan-induced thermal hyperalgesia (withdrawal latency, in seconds). Results are expressed

as the mean ± SEM of 6 mice per group. ***, *P*<0.001 versus control; two-way ANOVA followed by Bonferroni's test.

Supplementary Fig. 13. Anti-inflammatory effects of ARN272 0h and 4 h after intraplantar injection of carrageenan. Administration of ARN272 (mg-kg^{-1}, i.p.) reduced carrageenan-induced paw edema (volume, in ml). Results are expressed as the mean ± SEM of 6 mice per group. ***, *P*<0.001 versus control; two-way ANOVA followed by Bonferroni's test.

Supplementary Fig. 14. The CB_2 receptor antagonist AM630 and the transient receptor potential vanilloid-1 (TRPV-1) antagonist AMG9810 (each at 1 mg-kg^{-1}, i.p., 30 min before carrageenan) did not alter the antinociceptive effects of ARN272 (1 mg-kg^{-1}, i.p., injected together with carrageenan) on (**a**) thermal hyperalgesia and (**b**) paw edema. Results are expressed as the mean ± SEM of 6 mice per group.

Supplementary Fig. 15. Hypothetical model for the mechanism of action of FLAT. According to this model, extracellular anandamide is absorbed on the outer leaflet of the lipid bilayer and flips over to the inner leaflet, where it is desorbed by FLAT (1). FLAT carries the lipophylic transmitter through the cytosol, and delivers it to FAAH-1, which is exclusively found on intracellular membranes (2). FAAH-1 completes the deactivation of anandamide by catalyzing the hydrolysis of this compound to arachidonic acid (stick) and ethanolamine (ball) (3).

Methods

FLAT model

The α2 helix (residues 37 to 68) was removed from the crystal structure of FAAH-1-ΔTM (PDBid: 1MT5)[15] and positions 69 to 75 were modeled de novo. The co-crystallized ligand and water molecules were removed. Hydrogen atoms and missing heavy atoms were added. Side chains of residues 69-75, zero occupancy side chains, and polar hydrogen atoms were assigned the lowest energy conformations. Tautomeric states of histidines and the positions of asparagine and glutamine side chain amidic groups were optimized to improve the H-bond pattern.

Monte Carlo simulations

Conformational analysis of the α2-interacting loop was performed using the Metropolis Biased Probability Monte Carlo (BPMC) method as implemented in ICM3.7[40]. The initial temperature was set at 600 K. A total of $5x10^7$ energy evaluations were carried out. The variables sampled during the simulation were the backbone and side chain torsional angles of the loop amino acids. The side chain torsional variables of all the amino acids with at least one heavy atom within 2 Å from the loop were minimized together with the sampled variables before acceptance/rejection according to the Metropolis criterion.

Molecular dynamics simulations

Molecular dynamics simulations were conducted using the NAMD 2.6[41] software and the Amber99SB force field[42]. FLAT and FAAH-1-ΔTM were solvated in explicit solvent. The dimensions of the simulation box were chosen so to keep a margin of at least 8 Å from the solute in each coordinate direction, and the electro-neutrality of the cell was reached by adding counter-ions. The simulations were performed in the isobaric-isothermal statistical ensemble with periodic boundary conditions. Langevin dynamics was undertaken at the temperature of 300 K with a frictional coefficient of 5 ps^{-1} at the target pressure of 1 atm. A uniform time-stepping of 2 fs was used. Bonds involving hydrogen

atoms were restrained to their reference value. Short-range non-bonded interactions were calculated using a distance cutoff of 10 Å. Long-range electrostatic interactions were considered using the Particle Mesh Ewald method. The system was thermalized during 150 ps of molecular dynamics while smoothly releasing restraints initially applied onto the protein heavy atoms. The system was then allowed to evolve for a total simulated time of 100 ns.

Electrostatic simulations

The Poisson-Boltzmann equation was solved over a system in which FLAT was modeled as a polarizable solute and the solvent was modeled as a high-dielectric continuum plus an ionic strength of 0.145M. Electrostatic potential values generated by representative structures of FLAT and FAAH-1-ΔTM at the zeta nitrogen site of Lys^{142} were calculated and compared using the DelPhi software[43]. The simulations suggested that the α2 helix brings a positive electrostatic contribution to the lysine site. This contribution is the sum of the mere helix dipolar potential and the overall net charge potential generated by titratable residues borne by the α2 helix. In FLAT, this effect is only partially compensated by the reaction field generated by the solvent that replaces the α2 helix. The pKa shift between the two forms was estimated quantitatively by performing electrostatic calculations according to a conceptual thermodynamic cycle:

$$\Delta pKa = pKa(FLAT) - pKa(FAAH\ \Delta TM) = [(G_{FLAT}^{0} - G_{FLAT}^{+}) - (G_{\Delta TM}^{0} - G_{\Delta TM}^{+})]/(2.303RT)$$

This calculation provided a positive average pKa shift of about 0.8 pKa units, pointing to an increased probability of having a protonated catalytic lysine in FLAT.

Virtual ligand screening

Database selection and pre-filtering. 4,325,889 unique structures for virtual ligand screening (VLS) were retrieved from the Molcart database v.1.9.6 (Molsoft, La Jolla,

CA). First, compounds were filtered using the physicochemical profile expected of a potential transport inhibitor: molecular weight 300 - 400 Da, logP 4 - 8, H-bond donors 0 - 3, H-bond acceptors 2 - 4, polar surface area 20 - 80 $Å^2$, molecular volume 340 - 485 $Å^3$, ring terms 3 - 7. This profile was defined using 5 templates: i) anandamide; ii) AM404: iii) a reversible FAAH thiohydantoin inhibitor (compound 123 in [44]); iv) OL-92; and v) the leaving group of URB597. The first filtering step retained 288,307 compounds, which matched the sought physicochemical profile. Then, to avoid a bias toward known scaffolds, molecules within a Tanimoto distance between 0 and 0.6 (with 0 indicating that two molecules share an identical fingerprint generated according to the Daylight algorithm – Daylight Chemical Information Systems Inc., Laguna Niguel - CA) from any of the compounds i)-v) were discarded. At the end of the pre-filtering steps, 122,095 unique molecules were selected.

Docking procedure. The boundaries of the binding pocket were calculated using the Pocketome Gaussian Convolution algorithm as implemented in ICM3.7. The three-dimensional models of 122,095 molecules were automatically built and docked at the FLAT binding site according to the ICM3.7 standard docking procedure. This step identified 4,601 compounds that matched the energy criterion of -32 arbitrary score units.

Cluster analysis and visual inspection. The chosen compounds were submitted to an UPGMA chemical clustering procedure. The functional partition was selected at a threshold value of 0.5 Tanimoto distance. This returned 56 unique clusters. Depending on the cluster cardinality, one to three representatives were selected, providing 124 potential FLAT binders. After visual inspection 53 compounds were selected and 46, which were available from commercial vendors, were subjected to testing in vitro.

Chemicals

Anandamide, AM404, VDM-11, UCM-707, Win55212 and AMG9810 were purchased from Tocris (Ellisville, MO). λ-Carrageenan, AM251, AM630, PEG 400, and Tween-80 were from Sigma-Aldrich (Milan, Italy). ARN272 [(4-(5-(4-hydroxy-phenyl)-3,4-diaza-bicyclo[4.4.0]deca-1(6),2,4,7,9-pentaen-2-ylamino)-phenyl)-phenylamino-methanone] was from Ambinter (Paris, France). ARN272 was purified by liquid chromatography (LC) and its identity was confirmed by mass spectrometry (MS) and ^{1}H-nuclear magnetic resonance spectroscopy. Final purity was >95%. [^{3}H]-Anandamide, [^{3}H]-OEA, [^{3}H]-PEA and [^{3}H]-arachidonic acid were from American Radiolabeled Chemicals (Saint Louis, MO), and [^{3}H]-CP-55940 from Perkin Elmer (Boston, MA). [$^{2}H_4$]-Anandamide, [$^{2}H_4$]-OEA and [$^{2}H_4$]-PEA were from Cayman Chemicals (Ann Arbor, MI) and heptadecanoic acid was from NuChek Prep (Elysian, MN).

Neuronal cultures

Primary cultures of mouse and rat cortical neurons were prepared as described in[45].

FLAT cloning and expression

Rat FLAT mRNA was amplified by PCR using the following primers: forward, ACCATGGTGCTGAGCGAAGTGTGGACC; reverse, TCACGATGGCTGCTTTTGAGGGGT. An rFLAT amplicon was subcloned into the pCR®II vector using the TOPO® TA Cloning® kit (Invitrogen) and splicing was confirmed by sequencing. Amplicons of rat FAAH-1, FLAT and mutated FLAT-S170G were cloned into a pcDNA3.1 expression vector (Invitrogen) under the control of human cytomegalovirus promoter. Hek-293 cells were cultured in Dulbecco's-modified Eagle's medium (DMEM) supplemented with FBS (10% vol/vol) and transfected with Lipofectamine™ 2000 (10 μl, Invitrogen) containing 1 μg of plasmids. 18h after transfection, culture media were replaced with DMEM containing G418 (0.2 mg/ml, Calbiochem, San Diego, CA). After 4 weeks in culture, surviving clones were isolated and analyzed by Western blot to select cell lines stably expressing the transgenes.

Serine 173 in rat FLAT was mutated to glycine using the GeneTailor™ mutagenesis system (Invitrogen).

RT-PCR

RNA was extracted with TRIzol™, and cDNA synthesized from 1 μg of total RNA. PCR was conducted using the following primers: Forward, CATGGTGCAGTACGAGCTGTGG; Reverse, GGACTGGGGGACATTGGTATG. mRNA expression was determined using glyceraldehyde 3-phosphate dehydrogenase as standard.

Ribonuclease protection assays

Probes comprising nucleotides 20-309 of FAAH-1 and nucleotides 20-220 of FLAT were generated by PCR followed by subcloning into pCR®II vectors (Invitrogen). The constructs were linearized by digestion with BamH I and used as templates for in vitro transcription incorporated with ^{32}P-dCTP (MP Biomedicals, Solon, OH) using RNA polymerase SP6 (Roche). Ribonuclease protection assays were performed with an RPA III kit (Applied Biosystems, Austin, TX).

Southern blot analyses

Total RNA was extracted from tissues with TRIzol™ (Invitrogen). cDNA was synthesized from 20 μg of total RNA using SuperscriptII RNase H-reverse transcriptase (Invitrogen). cDNA was digested with BlpI and electrophoresed at 30V overnight. Southern blots were performed using a standard protocol[46] with a 5'-terminal probe (237bp, from 41-277bp) or a 3'-terminal probe (409bp, from 601-1010bp) for FAAH-1.

Western blots

Protein (20 μg) were subjected to electrophoresis on 4-15% SDS-PAGE gels and transferred onto Immobilon™ membranes (Millipore, Billerica, MA). Western blots were run using antibodies against V5 (1:3,000, Invitrogen), FAAH-1 (1:500, Abbiotec, San

Diego, CA) and β-actin (1:10,000, Calbiochem). Bands were visualized with an Electrochemiluminescence Plus kit (Amersham Biosciences). Quantitative analyses were performed using the National Institutes of Health Image software, using β-actin as an internal standard.

FLAT binding assays

A pGEX-rFLAT plasmid containing fused rat FLAT and GST was constructed into a pGEX-4T vector (Amersham Biosciences, Piscataway, NJ) and digested with BamH 1. The GST-FLAT fusion protein was generated in *E. coli* (BL21 strain, Novagen, San Diego, CA). After induction, bacteria were grown at 27°C for 10 h, and the protein purified using glutathione-sepharose beads (Amersham Biosciences). Purified GST-FLAT was incubated at 25°C for 2 h in HEPES buffer (50 mM, pH 7.0) containing KCl (50 mM), EDTA (5 mM), dithiothreitol (10 mM), and [^{3}H]-anandamide (15 Ci/mmol). Free [^{3}H]-anandamide was separated on a Sephadex G-25 spin column (Amersham Biosciences) and radioactivity in the bound fraction was measured. Non-specific binding was determined in the presence of non-radioactive anandamide (10 μM).

Anandamide translocation

Hek293 cells or cortical neurons in cultures were incubated for 5 min at 37°C in Tris–Krebs buffer (pH 7.5) containing [^{3}H]-anandamide or other [^{3}H]-labeled lipids (each at 200 nM; 10,000 dpm, specific activity 20 Ci/mmol). Cells were rinsed with Tris–Krebs, scraped into NaOH (0.2 N) and radioactivity was measured. Test compounds were added to the cultures 10 min before [^{3}H]-anandamide.

Anandamide release

Neuro-2A cells (1x10^6) were cultured overnight in 100-mm dishes and transfected with control vector or pcDNA3.1/rFLAT plasmid using Lipofectamine™ 2000 (Invitrogen) for 48 h. Media were harvested and proteins were removed with cold acetone. Supernatants were collected, and lipids extracted with methanol/chloroform (1:2, vol/vol) containing

[$^2H_4$]-OEA, [$^2H_4$]-anandamide and [$^2H_8$]-2-AG (100 pmol). After centrifugation at 1,500x*g* for 15 min, organic phases were collected and dried. Lipids were reconstituted in methanol (0.1 ml) and quantified by LC/MS[47].

Behavioral tests

We used male CD1 mice weighing 25–30 g (Charles River, Calco, Italy). The mice had free access to food and water and were maintained under a 12 h light/dark cycle at controlled temperature and relative humidity. Behavioral experiments were performed in accordance with the Ethical Guidelines of the International Association for the Study of Pain and approved by Italian regulations on protection of animals used for experimental and other scientific purposes (D.M. 116192) as well as with European Economic Community regulations (O.J. of E.C. L 358/1 12/18/1986). We injected formalin (5% in sterile saline, 10 µl) into the plantar surface of the left hind paw and nocifensive behavior (licking and biting of the injected paw) was monitored as described[48]. Edema was elicited by injecting λ-carrageenan (1% weight/vol, 20µl) into the left hindpaw of mice. Edema was measured with a plethysmometer (Ugo Basile, Comerio, Italy). Thermal hyperalgesia was assessed as described[49]. Vehicle or ARN272 were administered by i.p. (0.01-3 mg/kg) or intracerebroventricular (0.0-3 µg per animal) injection immediately before formalin or carrageenan. Antagonists were injected (1 mg-kg^{-1}, i.p.) 30 min before formalin or carrageenan.

Lipid measurements *ex vivo*

CD1 mice received i.p. injections of vehicle (5% polyethylene glycol 400-5% Tween-80 in saline, 5ml/kg) or ARN272 (1 mg/kg) and were killed 1-2 h later under isoflurane anaesthesia. Blood was collected through a left cardiac puncture and centrifuged at 3000x*g* for 30 min. Plasma (0.2 ml) was incubated with 1 ml cold acetone, centrifuged at 1,500x*g* for 15 min at 4ºC and suspended in 50% methanol (2 ml) containing [$^2H_4$]-anandamide, [$^2H_4$]-OEA, [$^2H_4$]-PEA and [$^2H_8$]-2-AG. Lipids were extracted with

chloroform (2 ml) and organic phases were collected and dried under nitrogen. Lipids were reconstituted in methanol (0.1 ml) and measured by LC/MS.

Statistical analyses

Results are expressed as the mean ± s.e.m of n separate experiments. The significance of differences between groups was evaluated by one-way analysis of variance (ANOVA) followed by a Dunnett's test for multiple comparisons, or a Student's *t*-test. For behavioral experiments, differences were evaluated by two-way ANOVA following by a Bonferroni's test. Analyses were conducted using the GraphPad Prism software (GraphPad Software, San Diego, CA), and differences were considered significant if $P < 0.05$.

Supplementary References

40. Abagyan, R. & Totrov, M. Biased probability Monte Carlo conformational searches and electrostatic calculations for peptides and proteins. *J Mol Biol* 235, 983-1002 (1994).
41. Phillips, J. C. et al. Scalable molecular dynamics with NAMD. *J Comput Chem* 26, 1781-802 (2005).
42. Hornak, V. et al. Comparison of multiple Amber force fields and development of improved protein backbone parameters. *Proteins* 65, 712-25 (2006).
43. Rocchia, W., Alexov, E. & Honig, B. Extending the Applicability of the Nonlinear Poissonâ^'Boltzmann Equation: Multiple Dielectric Constants and Multivalent Ions. *The Journal of Physical Chemistry B* 105, 6754-6754 (2001).
44. Seierstad, M. & Breitenbucher, J. G. Discovery and development of fatty acid amide hydrolase (FAAH) inhibitors. *J Med Chem* 51, 7327-43 (2008).

45. Evans, M. S., Collings, M. A. & Brewer, G. J. Electrophysiology of embryonic, adult and aged rat hippocampal neurons in serum-free culture. *J Neurosci Methods* 79, 37-46 (1998).
46. Pearson, G. D. & Mekalanos, J. J. Molecular cloning of Vibrio cholerae enterotoxin genes in Escherichia coli K-12. *Proc Natl Acad Sci U S A* 79, 2976-80 (1982).
47. Fu, J. et al. Food intake regulates oleoylethanolamide formation and degradation in the proximal small intestine. *J Biol Chem* 282, 1518-28 (2007).
48. Li, X. et al. Expression genetics identifies spinal mechanisms supporting formalin late phase behaviors. *Mol Pain* 6, 11 (2010).
49. Hargreaves, K., Dubner, R., Brown, F., Flores, C. & Joris, J. A new and sensitive method for measuring thermal nociception in cutaneous hyperalgesia. *Pain* 32, 77-88 (1988).

Supplementary Table 1. Intraplantar ARN272 does not cause nociceptive behavior.

	Vehicle	ARN272				AMG9810	Capsaicin (1.6 μg)	
							Vehicle	AMG9810
Dose (μg)	0	1	3	10	30	10	0	10
Licking (sec)	0	0	0	0	0	0	77.8±3.8	3.7±1.7***

Data present as mean ± S.E.M (n = 6 per group).

***, P<0.001 one-way ANOVA followed by Bonferroni's test.

Supplementary Figure 1

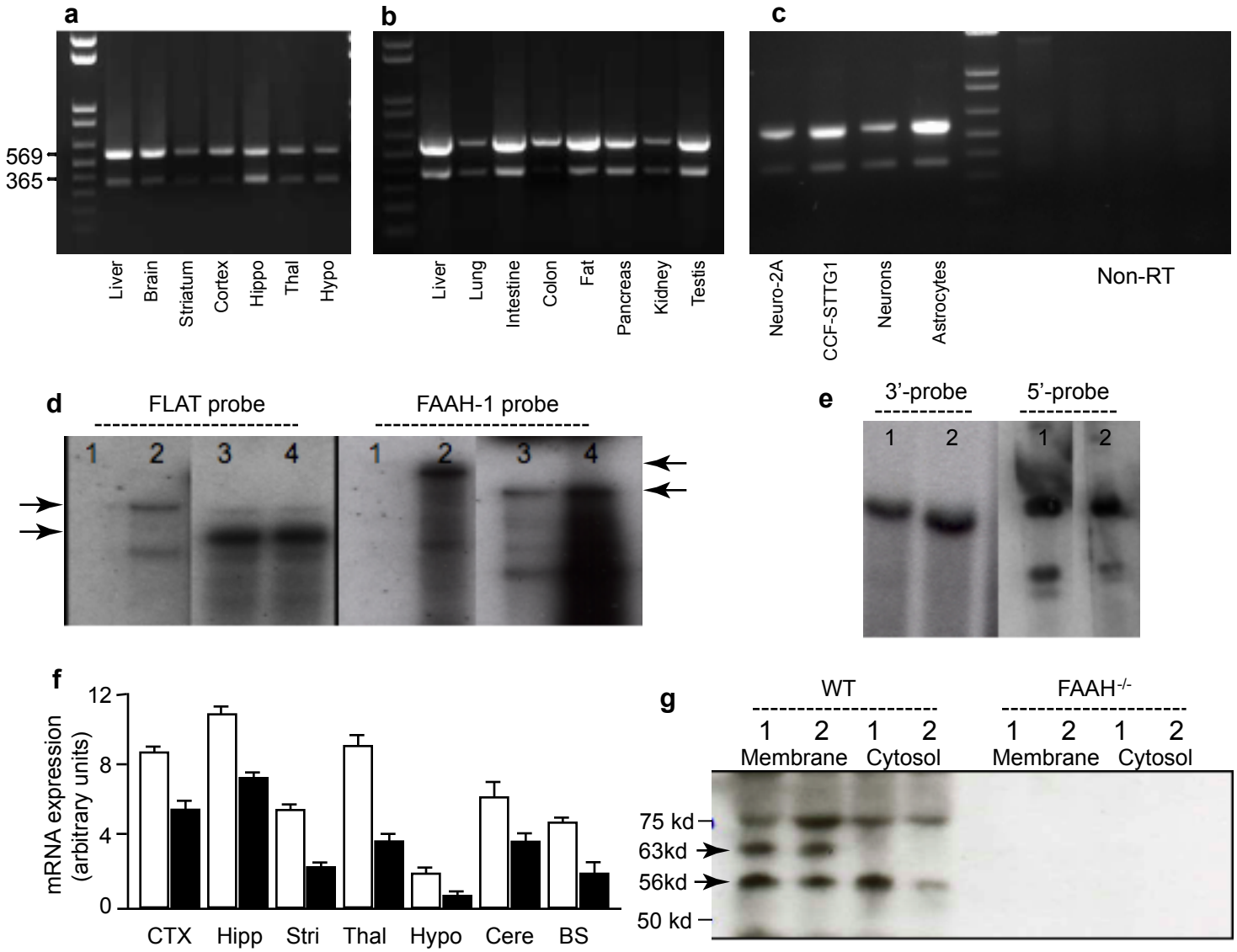

Supplementary Figure 2

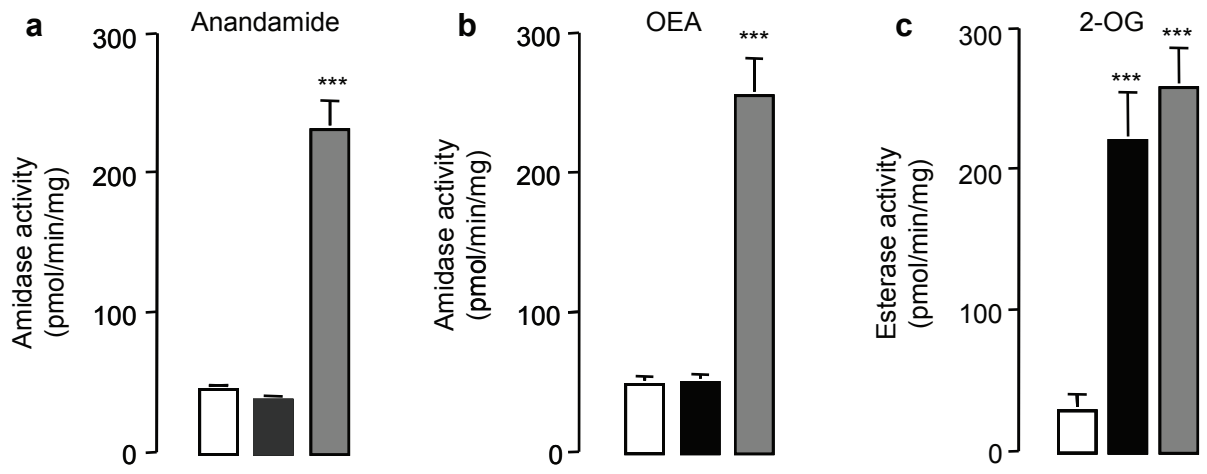

Supplementary Figure 3

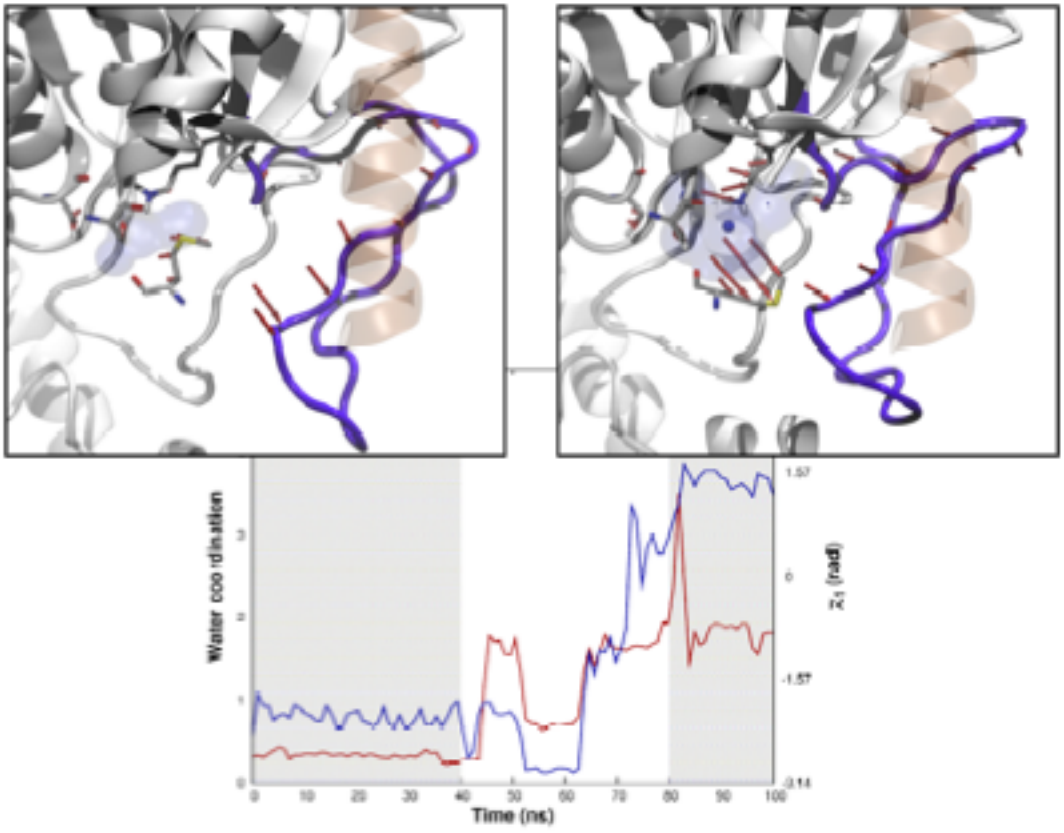

Supplementary Figure 4

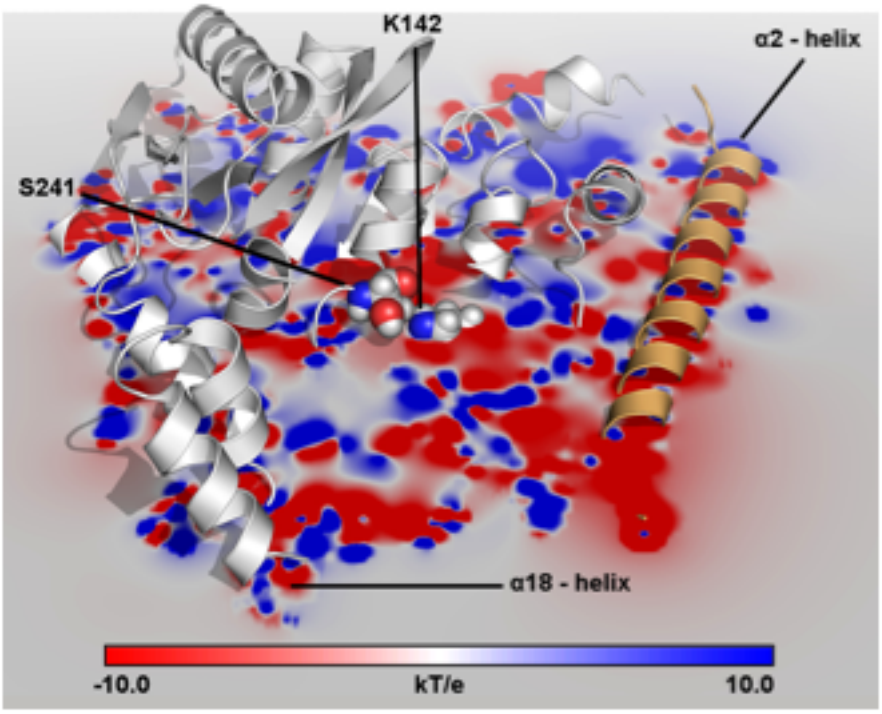

Supplementary Figure 5

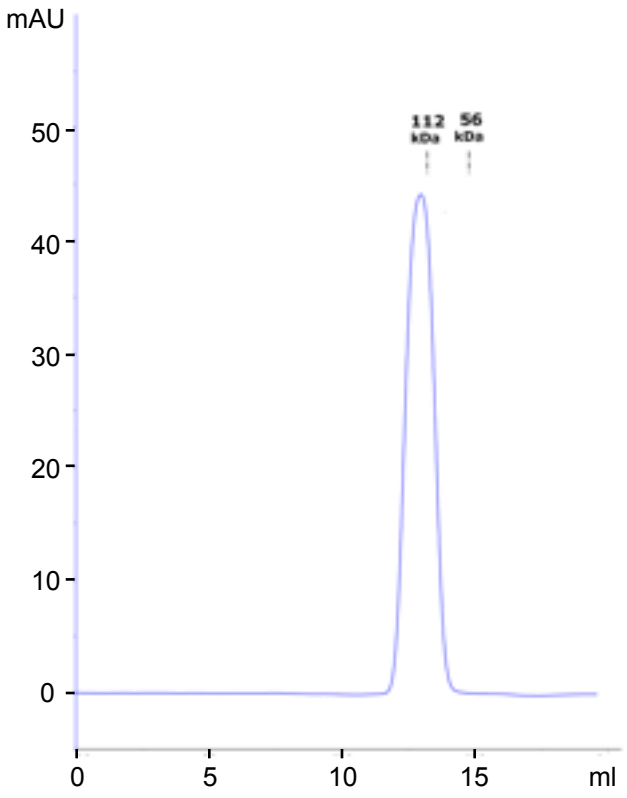

Supplementary Figure 6

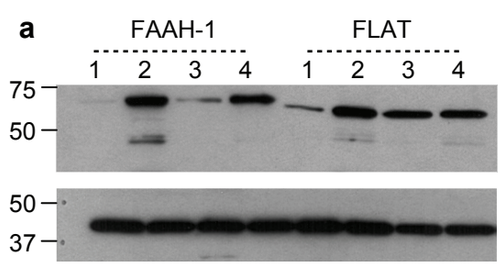

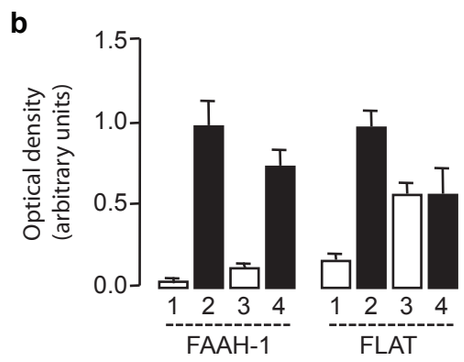

Supplementary Figure 7

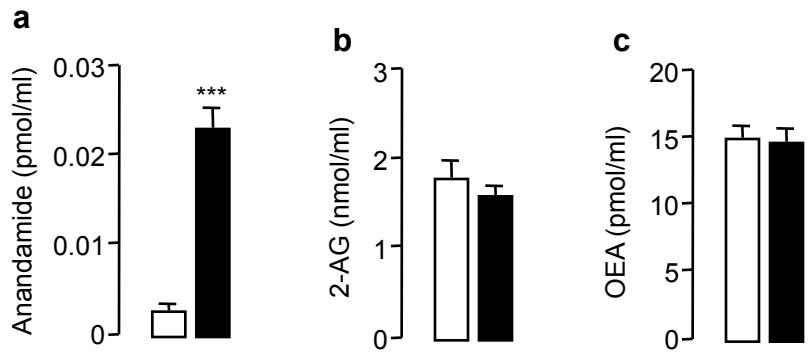

Supplementary Figure 8

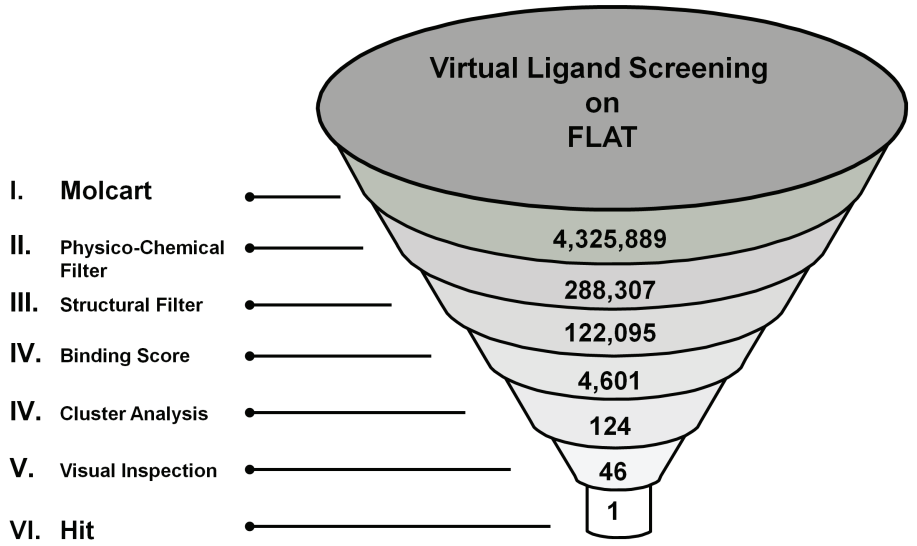

Supplementary Figure 9

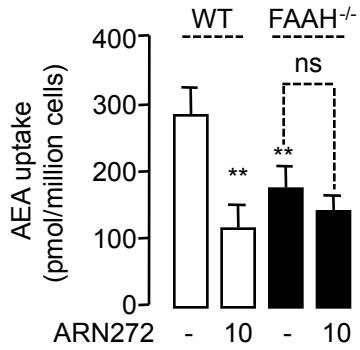

Supplementary Figure 10

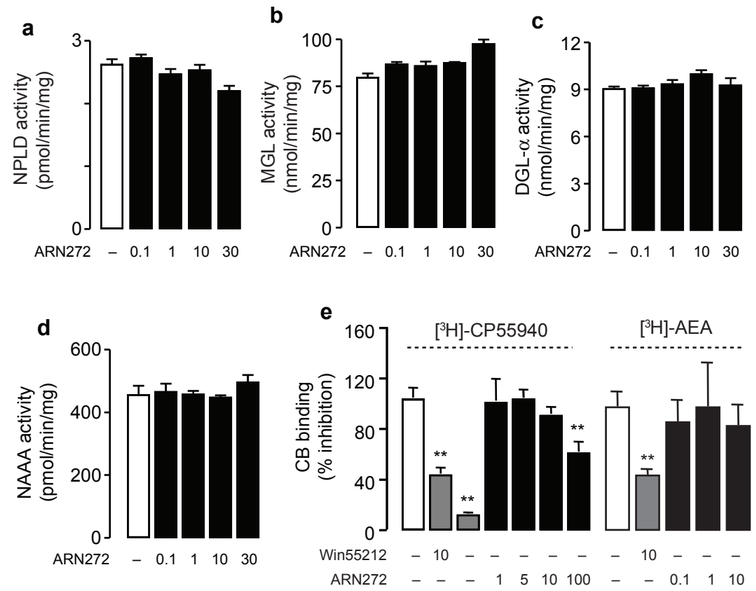

Supplementary Figure 11

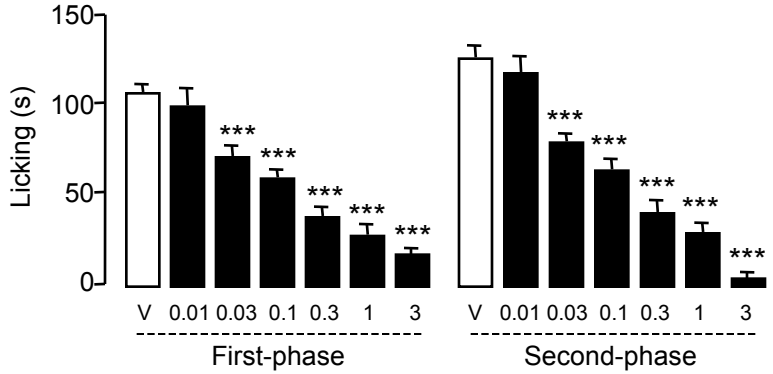

Supplementary Figure 12

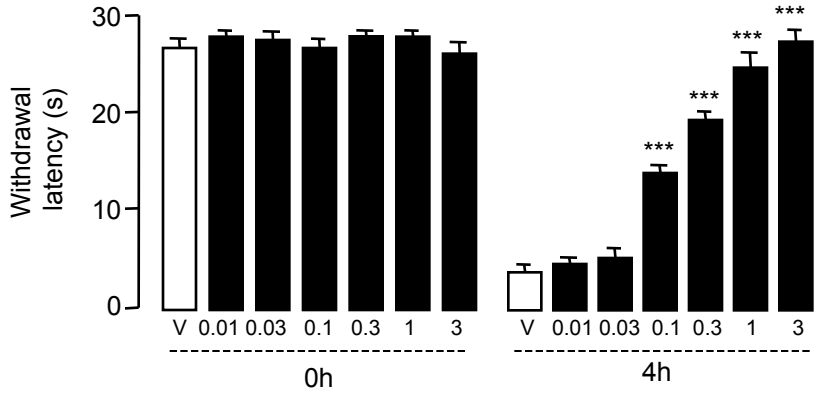

Supplementary Figure 13

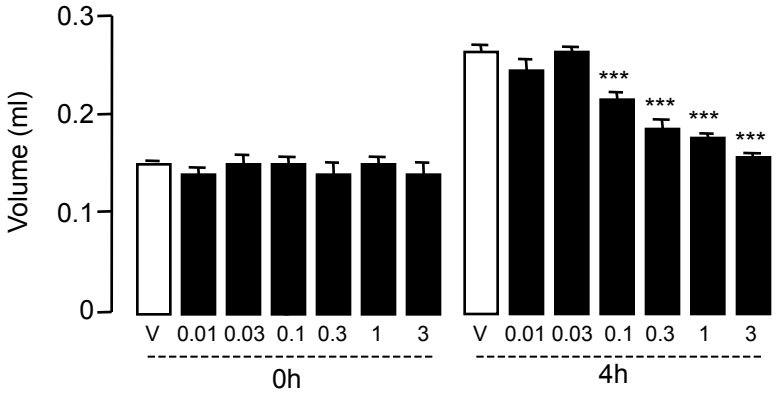

Supplementary Figure 14

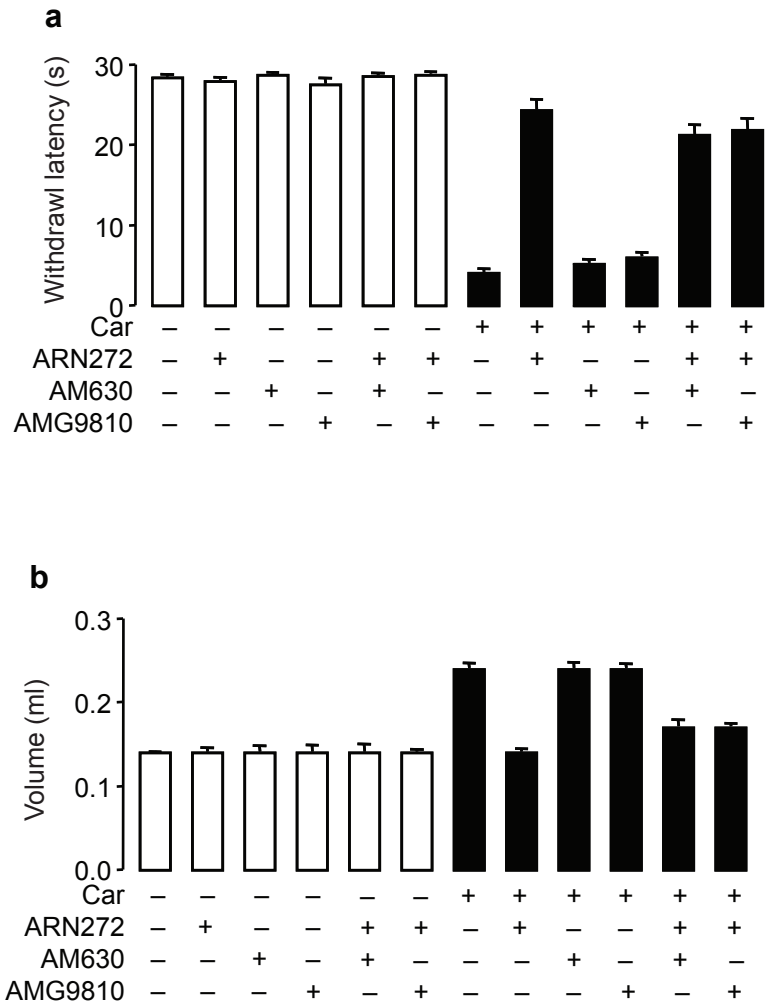

Supplementary Figure 15